Amplified Photoacoustic Performance and Enhanced Photothermal Stability of Reduced Graphene Oxide Coated Gold Nanorods for Sensitive Photoacoustic Imaging

Hyungwon Moon,[†] Dinesh Kumar,[‡] Haemin Kim,[§] Changbeom Sim,[†] Jin-Ho Chang,[§] Jung-Mu Kim,[⊥] Hyuncheol Kim,[*,†] and Dong-Kwon Lim[*,‡]

[†]Department of Chemical and Biomolecular Engineering and [§]Interdisciplinary Program of Integrated Biotechnology, Sogang University, 35 Baekbeom-ro, Mapo-gu, Seoul 121-742, South Korea, [‡]KU-KIST Graduate School of Converging Science and Technology, Korea University, 145 Anam-ro, Seongbuk-gu, Seoul 136-701, South Korea, and [⊥]Department of Electronic Engineering, Chonbuk National University, 567 Baeckje-daero, Jeonju 561-756, South Korea

ABSTRACT We report a strongly amplified photoacoustic (PA) performance of the new functional hybrid material composed of reduced graphene oxide and gold nanorods. Due to the excellent NIR light absorption properties of the reduced graphene oxide coated gold nanorods (r-GO-AuNRs) and highly efficient heat transfer process through the reduced graphene oxide layer, r-GO-AuNRs exhibit excellent photothermal stability and significantly higher photoacoustic amplitudes than those of bare-AuNRs, nonreduced graphene oxide coated AuNRs (GO-AuNRs), or silica-coated AuNR, as demonstrated in both *in vitro* and *in vivo* systems. The linear response of PA amplitude from reduced state controlled GO on AuNR indicates the critical role of GO for a strong photothermal effect of r-GO-AuNRs. Theoretical studies with finite-element-method lab-based simulation reveal that a 4 times higher magnitude of the enhanced electromagnetic field around r-GO-AuNRs can be generated compared with bare AuNRs or GO-AuNRs. Furthermore, the r-GO-AuNRs are expected to be a promising deep-tissue imaging probe because of extraordinarily high PA amplitudes in the 4−11 MHz operating frequency of an ultrasound transducer. Therefore, the r-GO-AuNRs can be a useful imaging probe for highly sensitive photoacoustic images and NIR sensitive therapeutics based on a strong photothermal effect.

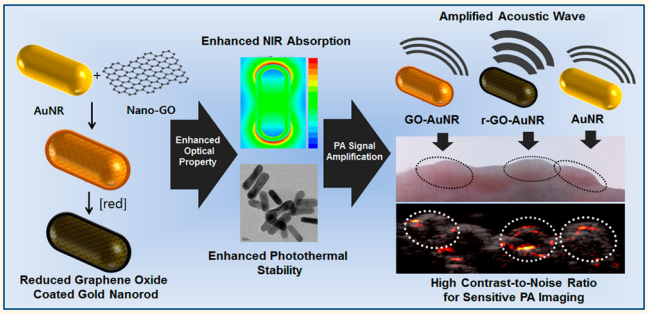

KEYWORDS: photoacoustic imaging · graphene-coated gold nanorods · photothermal effect

Recently, photoacoustic (PA) imaging has been highlighted as one of the latest and most promising biophotonic diagnostic modalities. This technique incorporates high spatial resolution, deep penetration depth, nonionizing radiation, noninvasive imaging techniques, and optically functionalized imaging.[1,2] Photoacoustic signals are generated by one of four different mechanisms: thermal expansion, vaporization, chemical reaction with photonics, or optical breakdown.[3] Among these four mechanisms, only thermal expansion has been demonstrated to be safe for biological applications.[3] When an optically absorbing compound is irradiated by laser pulses that are shorter than the thermal transport time of the absorbed energy, transient thermoelastic expansion occurs, and a subsequent PA pressure wave is generated within the compound.[4] During thermal expansion in an optical absorber, the conversion efficiency of light energy to a PA pressure wave is the most important factor to determine the intensity of the resultant optical contrast. This conversion efficiency also strongly influences the ability of the optical absorber to successfully reconstruct a sensitive PA image. Conversion efficiency is mainly determined by the light absorbance and the heat capacity of the optical absorber. However, thermal expansion

* Address correspondence to dklim@korea.ac.kr, hyuncheol@sogang.ac.kr.

Received for review November 16, 2014 and accepted March 4, 2015.

Published online March 09, 2015
10.1021/nn506516p

is the least efficient mechanism for generating PA signals; thus, the sensitivity of PA imaging is quite limited. To overcome this technical hurdle, exogenous PA contrast agents with high optical absorbance have been employed in efforts to improve PA imaging sensitivity.[5,6] A wide range of nanomaterials such as gold nanoparticles (AuNPs),[7] gold nanorods (AuNRs),[8] gold nanocages,[9] gold carbon nanotubes,[10] silica-coated AuNRs,[11] and carbon nanotubes[12] have been extensively studied as potential contrast agents for PA imaging. These agents were chosen based on their tunable, high absorption cross sections in the near-infrared (NIR) light spectrum and resulting strong photothermal effects. For heterogeneous PA imaging agents, the efficiency of heat transfer between two different materials was found to be a greatly important factor in obtaining amplified PA intensity as demonstrated by Emelianov *et al.*, using silica-coated AuNRs.[11,13] Therefore, developing new heterogeneous systems with excellent NIR light absorption properties and an efficient heat transfer mechanism is strongly required, and these can be promising imaging agents for achieving a sufficiently high contrast-to-noise ratio (CNR) to enable high-resolution PA imaging with minimized possible side effects.

RESULTS AND DISCUSSION

Here we describe a novel approach for significantly increasing the amplitude of PA signals. In our approach, gold nanorods are encapsulated within an optically absorbing shell material, reduced graphene oxide (r-GO). The ability of the graphene shell to amplify the PA signal demonstrates the enhanced NIR light absorption of the heterogeneous system and greatly decreased heat transfer resistance from the gold nanoparticles to the ambient signal-generating medium. To investigate the effect of the GO redox state on the amplification of the PA signal, we prepared chemically or optically reduced GO-coated AuNRs (r-GO-AuNRs) (Figure 1A).

Chemical and Optical Methods for the Preparations of r-GO-AuNRs. The GO coating procedure was performed as previously described.[14] Briefly, cetyltrimethylammonium bromide (CTAB)-AuNRs were prepared *via* the seed-mediated growth method.[15] The nanosized GO solution (<100 nm) was prepared using a modification of Hummers' method.[16,17] Positively charged AuNRs (aspect ratio: 3.5) were dropped into the nanosized GO solution, which was negatively charged, thereby producing graphene oxide (GO)-coated gold nanorods through simple electrostatic interactions (Figures 1A, S1).[14] For the preparation of r-GO-coated AuNRs, two different methods were employed. These two methods included a chemical method using hydrazine monohydrate[18] and a visible light (Xe lamp)-induced method[19] (Figure 1A). For the chemical method, 1.0 mL of GO-AuNR solution was reacted at 95−100 °C in the presence of 10 μL of ammonia solution (28%) and 5.0 μL of hydrazine monohydrate ($NH_2NH_2-H_2O$). To determine the optimum conditions for preparing r-GO-coated AuNRs in the context of PA signal generation and particle stability, the chemical reduction time was varied from 10 to 120 min. For the visible-light-induced method, 10 mL of GO-AuNR solution was irradiated for 120 min using a Xe lamp (1.56 W/cm^2, 400−780 nm) in the presence of 100 μL of ammonia solution (28%); the temperature was maintained at 25 °C (Figure S2). In both reactions, the solution changed color from pale yellow-brown to dark brown as the reaction progressed and GO was converted to r-GO. After completion of the reactions, the particles were centrifuged two times at 15000*g* for 15 min to remove the reagents (hydrazine or ammonia) and then resuspended in distilled water.

High-resolution TEM (HR-TEM) images, UV−visible spectra, X-ray diffraction analysis (XRD), and Raman analysis all demonstrated the successful formation of r-GO-AuNRs (Figures 1B−D, S3). The GO layer on the AuNRs was not easily visualized in the HR-TEM images (Figure 1B); however, after reduction, a few layers of r-GO surrounding the surfaces of the AuNRs (2.5 nm) prepared by either method were clearly visible (Figure 1B). The presence of the GO layer on the AuNRs was confirmed by monitoring the presence of the characteristic peak at 230 nm, as shown in a typical UV−visible spectrum (Figure 1C, red line).[20] The UV−visible spectra also showed the appropriate red-shifted absorption peak [from 230 nm (GO) to 270 nm (r-GO)] and the longitudinal plasmonic band of the AuNRs (around 750 nm), which indicates that the electronic state of the sp^2 bond was recovered without inducing significant particle aggregation.[21] Increasing the reaction time from 60 min to 120 min (Figure 1C, orange line) resulted in decreased absorption at 270 and 750 nm, which indicates partial aggregation of the r-GO-AuNRs. This aggregation may be due to the increase in hydrophobicity as the hydrophilic functional groups (*i.e.*, hydroxy, epoxide, and carboxylic acid) are gradually reduced.[21] The r-GO-AuNR solution (green line) prepared with a Xe lamp also showed the characteristic r-GO peak at 270 nm and the longitudinal plasmonic band of the AuNRs around 750 nm. These peaks indicate the successful formation of r-GO and the absence of any damage to the rod-shaped particle structures. Plasmonic light absorption by the AuNRs (peak absorption; 520 nm, 750 nm) was expected to play an important role in maintaining the reduced state of r-GO on the AuNRs.[22] Importantly, the optical-based reduction method, which did not use any toxic chemical reagents to generate the r-GO-AuNRs, is especially useful for generating nontoxic *in vivo* imaging materials.[23] The reduced state of GO was further examined using XRD and Raman analysis. The characteristic GO peak (at 10.02°) in the GO-AuNR

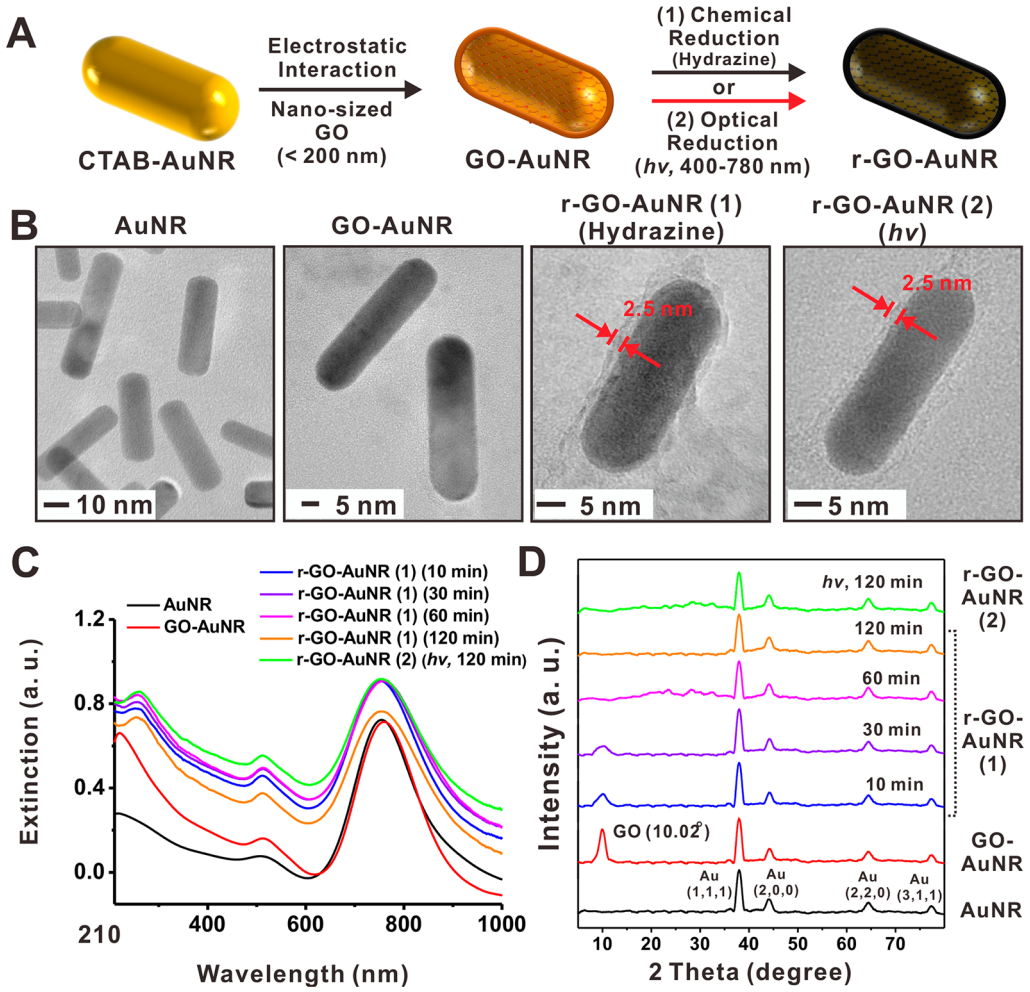

Figure 1. Synthesis and characterization of r-GO-AuNRs. (A) Overall synthesis schemes of GO-AuNRs and r-GO-AuNRs (1) using the chemical method (with hydrazine) and r-GO-AuNRs (2) using the visible-light-induced method (using a Xe-lamp). (B) HR-TEM images of AuNRs, GO-AuNRs, r-GO-AuNRs (1), and r-GO-AuNRs (2). (C) UV− visible spectra. (D) XRD spectra of AuNRs (black line), GO-AuNRs (red line), and r-GO-AuNRs (1) that had been reacted with hydrazine for 10 or 120 min and of r-GO-AuNRs (2) that had been illuminated with visible light for 120 min.

XRD spectra gradually disappeared as the reaction time increased (Figure 1D).[24] Similarly, r-GO-AuNRs prepared with visible light did not exhibit the characteristic GO peak. Raman analysis revealed that the I_D/I_G ratio gradually increased as the reaction time increased. The ratios were 0.92 (GO-AuNRs alone), 1.14 (10 min reaction), 1.16 (30 min), 1.18 (60 min), and 1.17 (120 min) (Figure S3). Importantly, the I_D/I_G ratio of r-GO-AuNRs prepared with visible light was 1.17, which indicates that r-GO was successfully formed.[24,25]

Photoacoustic Performances of r-GO-AuNRs. Next, the PA imaging performance of the AuNRs, GO-AuNRs, and r-GO-AuNRs (1) prepared with the chemical method (reaction time, 60 min) and the r-GO-AuNRs (2) prepared with the optical method were investigated. First, a pulsed laser with variable wavelength (680−800 nm) was used, and an input laser with a power of 4.2−8.2 mJ/cm^2 was used. Particle solutions (100 μL, 2.5 nM) were placed in NIR-inactive Tygon tubes (inner diameter, 0.127 cm). The PA signals detected by the linear array transducer (operating frequency, 5−14 MHz) were then used for PA image reconstruction (Figure S4). Representative PA images of the four samples at 700 and 800 nm are shown in Figure 2A. Both preparations of r-GO-AuNRs exhibited stronger PA signal intensities compared with the AuNRs and the GO-AuNRs, as confirmed by a quantitative comparison of the PA signal intensities of the sample solutions (Figure 2B). Despite the presence of the GO layer on the GO-AuNRs, the GO-AuNRs showed almost identical PA signal amplitudes (au) to those of the bare AuNRs in all investigated ranges of input laser power (GO-AuNRs, 26.49 ± 0.77; AuNR, 25.27 ± 0.56; 6.2 mJ/cm^2). More importantly, the chemically reduced r-GO-AuNRs (1) (blue line) showed the highest PA signal amplitude (53.77 ± 1.71 at 6.2 mJ/cm^2), which was 2 times higher than the PA signal intensity of the bare AuNRs. The PA signal amplitude of the r-GO-AuNRs (2) (green line) was 46.77 ± 0.61 at 6.2 mJ/cm^2, which was slightly lower

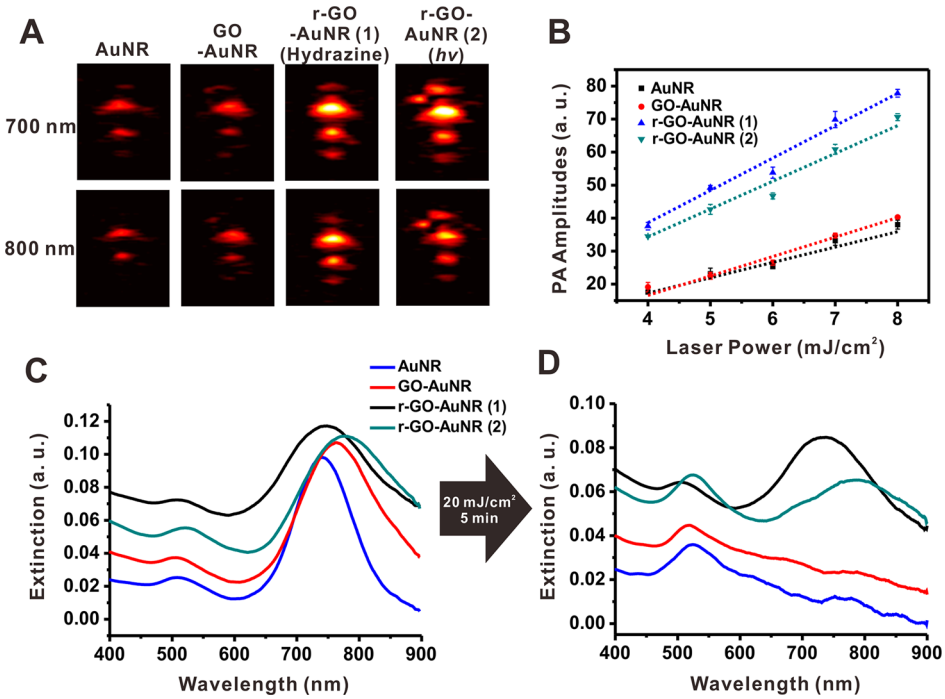

Figure 2. Photoacoustic amplitudes and photothermal stabilities of AuNRs, GO-AuNRs, r-GO-AuNRs (1), and r-GO-AuNRs (2). (A) Representative PA images obtained using excitation wavelengths of 700 and 800 nm (input laser power, 6.2 mJ/cm^2; pulse rate, 10 Hz). (B) Photoacoustic amplitudes obtained with different laser power inputs. (C, D) UV−visible spectra of AuNRs (blue line), GO-AuNRs (red line), r-GO-AuNRs (1) (black line), and r-GO-AuNRs (2) (dark cyan line) before (C) and after (D) laser illumination for 5 min (20 mJ/cm^2, 10 Hz).

than that of the r-GO-AuNRs (1). This difference may be due to the smaller amount of r-GO in the optically reduced r-GO-AuNRs (2). The PA signal intensities of all particle solutions increased linearly as the input laser power increased from 4.2 to 8.2 mJ/cm^2. Importantly, the PA signal intensities of the r-GO-AuNRs (1) at 4.2 mJ/cm^2 input laser power were still strong enough to produce high-contrast PA images. When irradiated under high laser power, some overheated agents are known to form bubbles and generate thermal explosions, which can cause cellular damage.[10] Therefore, achieving adequate PA signal amplitudes of imaging agents with low input laser energy is highly desirable for sensitive *in vivo* PA imaging applications, because the low input laser energy can minimize damage to normal tissues by laser or imaging agents.[10] Moreover, the strong PA signal intensities generated by the r-GO-AuNRs can dramatically reduce the minimum concentration required for PA-based diagnoses. For example, 0.5 nM r-GO-AuNRs was sufficient to generate a detectable PA signal; in contrast, this signal intensity was only achieved with a 4-fold greater concentration of AuNRs alone (2.0 nM) (Figure S5). In addition to generating a strong PA signal amplitude, the PA imaging agent must also be photothermally stable in order to perform consistent optical absorption and to generate an adequate photoacoustic response.[13] We investigated the photothermal stability of each particle type under continuous radiation generated by a pulsed laser (750 nm, 20 mJ/cm^2, 10 Hz repetitions, 5−7 ns laser pulses) for 5 min. The changes in the UV−visible spectra and particle shape were then monitored (Figures 2C, S6). After 5 min, the UV−visible spectra of the AuNRs (blue line) exhibited a completely collapsed plasmonic band at 750 nm, which is indicative of low photothermal stability under the conditions tested. On the other hand, the r-GO-AuNRs (1) (black line) did not show any significant change in the plasmonic band at 750 nm in the UV−visible spectra (Figure 3C). Furthermore, no morphological changes of the r-GO-AuNRs were observed by TEM (Figure S6), demonstrating that the r-GO-AuNRs (1) exhibit excellent photothermal stability. The optically produced r-GO-AuNRs (2) showed inferior photothermal stability compared with the chemically reduced particles, probably due to incomplete reduction of the GO. The excellent thermal conductivity of the r-GO layer on the AuNRs is expected to play a critical role in maintaining their structure.[26−28] Cumulatively, these results indicate that r-GO-coated AuNRs exhibit superior optical properties compared with both bare AuNRs and GO-coated AuNRs.

To further investigate the optical and chemical properties of the r-GO-AuNRs and thus better understand the mechanisms by which they amplify PA signals, we investigated the PA signal intensity as a function of incident wavelength (680−800 nm) and as a function of the amount of GO reduction on the AuNRs that were produced with the chemical method (Figure 1C,D). As shown in Figure 3A, the PA signal

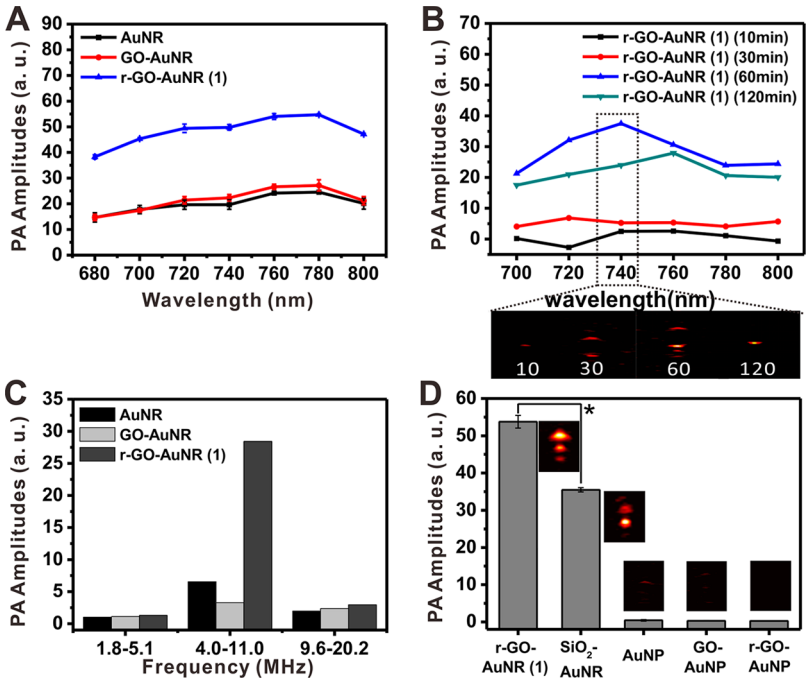

Figure 3. (A) Photoacoustic amplitude dependency on wavelength for AuNRs, GO-AuNRs, and r-GO-AuNRs (1). (B) Variations in PA signal amplitude resulting from alteration of the degree to which the GO is reduced. Chemically reduced r-GO-AuNRs were generated using different reaction times (10, 30, 60, and 120 min). (C) Photoacoustic amplitudes of AuNRs, GO-AuNRs, and r-GO-AuNRs (1) obtained using ultrasound transducers with different frequencies (2−5, 5−14, and 8−40 Hz). (D) Photoacoustic amplitudes of r-GO-AuNRs (1), silica-coated AuNRs (SiO_2-AuNR, 6 nm thickness), AuNPs, GO-AuNPs, and r-GO-AuNPs. Inset: PA images of each nanoparticle. Data are expressed as mean ± standard deviation ($N = 3$, $p < 0.05$).

intensity gradually increased as the incident wavelength increased from 680 to 780 nm. This range matches well with the longitudinal plasmonic resonance mode of the AuNRs. The degree of reduction of the GO on the AuNRs was also found to be important for successful amplification of the PA signal (Figure 3B). Short chemical reaction times (*i.e.*, 10 or 30 min) resulted in incomplete GO reduction, which subsequently led to low amplification of PA signals. In contrast, a 60 min (blue line) reaction of the r-GO-AuNRs resulted in the highest amplification of the PA signal. Representative PA images (inset) obtained from a 740 nm incident wavelength demonstrate the strong PA intensity achieved with r-GO-AuNRs that had been reduced for 60 min. Due to partial aggregation of the r-GO-AuNRs, which was observed at long reaction times (120 min), r-GO-AuNRs that had been reacted for 120 min showed decreased PA signal intensity (dark cyan line in Figure 3B). This observation is consistent with the UV−visible spectra (Figure 1C) and the previously reported optimum reaction time for chemical reduction.[21]

Since specific bandwidth frequencies have been shown to be important for achieving imaging sensitivity in different organs (*i.e.*, 1.8−5.1 MHz for the abdomen region, 4.0−11.0 MHz for the breast, and 9.6−20.2 MHz for the musculoskeletal anatomy and carotid artery),[29] we investigated the PA signal amplitudes of r-GO-AuNRs obtained with three different kinds of transducers. These transducers operated at distinct frequency ranges (2−5, 5−14, and 8−40 MHz), thus enabling the detection of the optimum acoustic signal frequency for achieving high sensitivity in PA imaging with r-GO-AuNRs (Figure 3C). No noticeable PA signal was observed from any particle solution, regardless of whether a low-frequency (2−5 MHz) or high-frequency (8−40 MHz) transducer was used. However, the r-GO-AuNRs exhibited maximum signal intensity at the 5−14 MHz operating frequency range. The signal intensity at this range was 36.9 times and 9.6 times higher than the intensities achieved with the 2−5 MHz and the 8−40 MHz operating frequency ranges, respectively. At the 5−14 MHz frequency range, the signal intensity of the r-GO-AuNRs was approximately 3 times higher than the intensities of both the AuNRs and the GO-AuNRs. In the context of clinical applications, the strong response obtained at the 5−14 MHz frequency is very important for the visualization of organs located deep within the body. For example, it is well known that low-frequency radio waves can penetrate deep into the body; however, these waves result in limited resolution, both in ultrasound (US) and PA imaging techniques. Therefore, the generation of strong acoustic waves at low frequency is highly desirable for achieving good sensitivity in PA imaging. Hence, we anticipate the r-GO-AuNRs described here to be a promising PA imaging agent that can enable sensitive diagnoses that require the imaging of organs

located deep within the body, such as detecting breast cancer in its early stages, through a combination of PA and US imaging.

Two main factors are likely to be responsible for the enhanced PA amplitudes achieved with the r-GO-AuNRs. The first factor is the thermally conductive r-GO layer, which enables highly efficient heat transfer. The second factor is the AuNRs, which enhance the light-absorbing properties of the r-GO. As reported by Emelianov *et al.*, the thin silica layer on the AuNRs greatly reduces the thermal resistance between materials, resulting in enhanced signal amplitudes in PA imaging.[13] Considering the excellent thermal conductivity of r-GO compared with silica (SiO_2), r-GO was hypothesized to be a desirable material for obtaining enhanced PA signal amplitudes because of increased light absorption properties and excellent thermal conductivity as well as reducing interfacial thermal resistance, which has not been systemically demonstrated yet. To verify this hypothesis and determine the plasmonic contributions to the amplified PA signals generated by the r-GO-AuNRs, we rigorously compared the amplitudes of the PA signals generated by silica-coated AuNRs (6 nm SiO_2 thickness) (Figure S7), AuNPs (30 nm, λ_{max} = 520 nm), GO-AuNPs, and r-GO-AuNPs. All of the rods and particles had the same optical density (OD; 1.0). Silica-coated AuNRs were prepared as previously described.[11] Positively charged, 30 nm AuNPs prepared using cysteamine were used to produce GO-AuNPs and r-GO-AuNPs (Figure S8). As shown in Figure 3D, silica-coated AuNRs showed lower PA signal amplitudes compared with those generated by the r-GO-AuNRs ($p < 0.05$). Silica-coated AuNRs are a relatively new PA contrast material and were designed to amplify PA signal intensity by decreasing the thermal resistance between the medium and the metallic AuNRs.[11] However, the excellent thermal conductivity (~5000 W/mK)[30] and the low thermal resistance of the r-GO on the AuNRs enabled the generation of even stronger PA signal amplitudes. Importantly, the AuNPs, GO-AuNPs, and r-GO-AuNPs showed only negligible PA signal intensities due to the lack of plasmonic absorption at 750 nm, the wavelength used for excitation (Figure 3D). Thus, we infer that the excellent thermal conductivity of the r-GO layer and the increased light absorption properties of the plasmonic nanoparticles enable the r-GO-AuNRs to generate enhanced PA signal intensities.

Finite-Element-Method Lab-Based Simulation Studies. To verify our experimental results using an orthogonal approach, we performed two different types of finite-element-method (FEM) lab-based simulations using Ansoft HFSSTM software (Ansys Inc., USA) for electromagnetic (EM) field distribution and heat transfer rate. As shown in Figure 4A–C, the EM fields were strongly distributed around both ends of the AuNRs. The peak values of the enhanced EM fields (E/E_{in}) of the AuNRs, GO-AuNRs, and r-GO-AuNRs were calculated to be 12.7, 36.1, and 53.8, respectively. The EM fields of the r-GO-AuNRs were 4 times stronger than those of the bare AuNRs, a finding that is consistent with the enhanced photothermal effect of the r-GO-AuNRs[14] and the increased PA amplitudes. On the other hand, simulations with spherical gold nanoparticles (AuNPs, GO-AuNPs, and r-GO-AuNPs) revealed only negligible EM fields (Figure 4D–F), most likely due to the lack of plasmonic resonance at 750 nm. The results for EM field distribution highlight the importance of efficient light absorption properties in obtaining enhanced PA amplitudes.

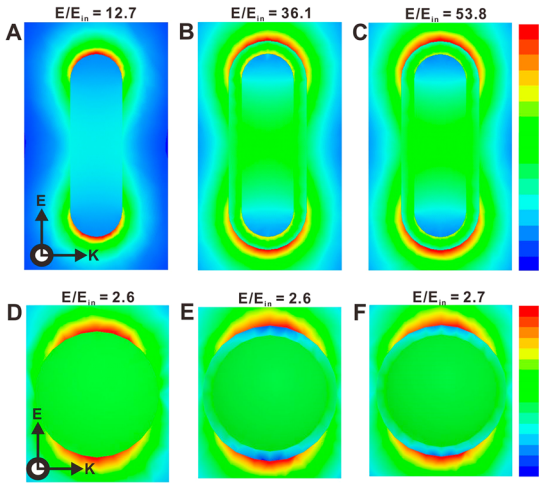

Figure 4. FEM lab-based simulations of (A) AuNRs, (B) GO-AuNRs, (C) r-GO-AuNRs, (D) AuNPs (30 nm), (E) GO-AuNPs (30 nm), and (F) r-GO-AuNPs (30 nm) obtained using an incident excitation wavelength of 750 nm (E/E_{in} indicates the peak values of the electromagnetic field distributions when light was applied (750 nm)). The higher field distributions (red colored) were produced as a result of the higher light absorption properties of nanoparticle depending on the their structures and types of material (*i.e.*, r-GO AuNPs showed significantly low field distributions because of the lack of light absorption in the 750 nm wavelength). These results show that one possible reason for the enhanced PA amplitude of r-GO-AuNRs is the higher light absorption properties of r-GO-AuNRs compared with other structures.

Heat transfer rate is also believed to be a critical factor that can significantly affect the thermal expansion-based acoustic wave. To understand the effect of heat transfer rate, we performed another FEM lab-based simulation by adopting the Poynting vector (Figure S9). As shown in Figure S9, the heat transfer rate in r-GO-AuNRs was 10 times higher than that of SiO_2-AuNRs and 2.5 times higher than that of GO-AuNRs because of the excellent thermal conductivity of r-GO. These results are well matched with the results of EM field distributions and the experimental results. These two simulation results indicate the use of r-GO as an additional coating layer is a desirable method to obtain enhanced PA amplitudes without increasing the nanoparticle concentration or changing the dimensions of the nanoparticle.

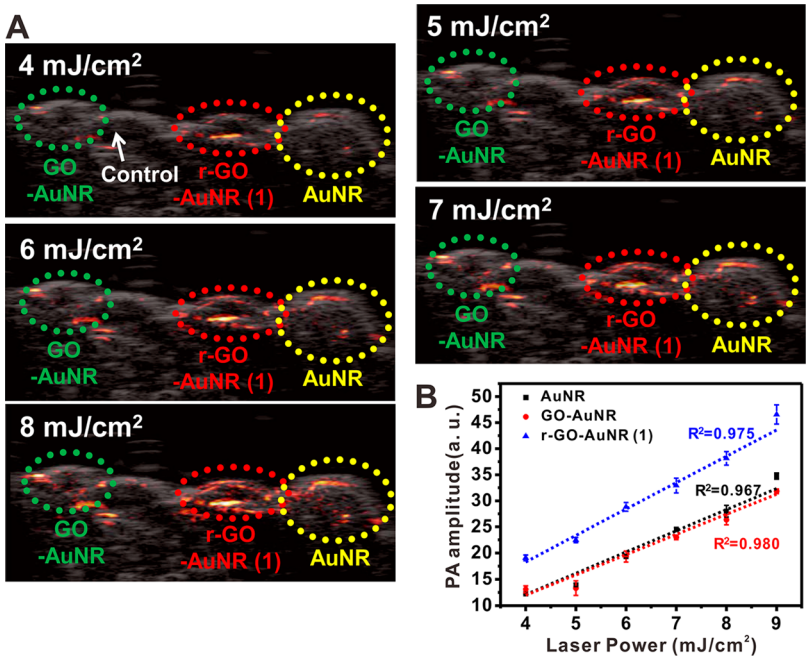

Figure 5. Photoacoustic images of AuNRs, GO-AuNRs, and r-GO-AuNRs (1) in live mice. (A) Subcutaneously injected Matrigel mixed with AuNRs, GO-AuNRs, or r-GO-AuNRs (1) was visualized after illumination with different input laser powers that ranged from 4 to 8 mJ/cm^2. Ultrasound (gray) and photoacoustic (red) images were overlaid with one another. (B) Quantitative analysis of photoacoustic signal intensities obtained with AuNRs (black), GO-AuNRs (red), and r-GO-AuNRs (1) (blue). The input laser power ranged from 4 to 8 mJ/cm^2. Data are expressed as mean ± standard deviation (N = 3).

Evaluations of the PA Performance of r-GO-AuNRs in an Animal Model. To investigate whether r-GO-AuNRs can be used as a PA contrast agent for high-sensitivity *in vivo* imaging, AuNRs, GO-AuNRs, or r-GO-AuNRs (1) were mixed with Matrigel (BD Biosciences, CA, USA) and then subcutaneously injected into the backs of mice (Figure S10). For the nanorod suspensions, 50 μL of AuNRs, GO-AuNRs, or r-GO-AuNRs (2.5 nM) was mixed with Matrigel (50 μL) at a 1:1 (v/v) ratio (*i.e.*, the final concentration of AuNRs was 1.25 nM). After injecting the sample and Matrigel mixture (100 μL) or Matrigel alone as a control into the backs of mice (Figure S10), the mixtures solidified within 1 min, thereby generating tissue-mimicking phantoms. To minimize experimental variation, all samples were imaged simultaneously at a fixed wavelength (750 nm) with varying laser powers (4.0 to 9.0 mJ/cm^2). The pulse duration was 5−7 ns, and the repetition rate was 10 Hz. Ultrasound images were first obtained to locate the sample positions; then, these images were superimposed with photoacoustic images (Figure 5A). Matrigel alone showed no noticeable acoustic signal intensity, even with a laser power of 9.0 mJ/cm^2. On the other hand, the PA signal intensities from the nanorod samples increased linearly as the incident laser power increased (Figure 5B). Most importantly, the r-GO-AuNRs exhibited the highest PA signal intensities of all of the samples (AuNRs: 19.34 ± 0.30, GO-AuNRs: 19.34 ± 1.03, and r-GO-AuNRs: 28.81 ± 0.84; 6.0 mJ/cm^2 incident laser power). This finding was consistent with our *in vitro* experiments. Even when using less than 4.0 mJ/cm^2 of incident laser power, the PA signal of the r-GO-AuNRs was clearly detected at the injection site, whereas neither the AuNRs nor the GO-AuNRs exhibited any signal stronger than the background noise. The minimum effective concentration of single-wall carbon nanotubes required for effective *in vivo* PA imaging has been reported to be 50 nM.[12,27] Thus, the 40-fold higher PA signal amplitudes achieved with the r-GO-AuNRs in this study represent a significant advance in high-resolution PA imaging, with many potential clinical diagnostic applications. Moreover, the r-GO-AuNRs enabled a clear visualization of the boundary of the tissue-mimicking phantom, even under low laser power (Figure 5A, red circle). Thus, the r-GO-AuNRs have great clinical potential for highly accurate surgical treatment of tumors. Additionally, the exquisite sensitivity of the r-GO-AuNRs can dramatically reduce both the minimum laser power required and the amount of agent required in order to achieve successful imaging.

CONCLUSIONS

In summary, we demonstrated that reduced graphene oxide-coated AuNRs are a promising photoacoustic imaging agent. These nanorods not only amplify the PA signal intensity but also exhibit excellent optical stability. We found that the amplified PA signals achieved with the r-GO-AuNRs were highly dependent on the reduced state of the GO and the presence of AuNRs. These findings

were demonstrated by determining the PA signal amplitudes over time as the amount of reduced GO-coated AuNR was varied and also by experimental and theoretical comparative studies with AuNPs. These r-GO-AuNRs are anticipated to be an extremely promising theranostic agent due to the following reasons: (1) they exhibit an enhanced photothermal effect,[6,14] (2) the r-GO layer exhibits a relatively straightforward surface chemistry [*via* covalent or noncovalent (*i.e.*, $\pi-\pi$ bonds or hydrophobic interactions) modifications of the ligand on the r-GO layer, which is essential for drug delivery systems],[31] and (3) they exhibit significantly amplified PA signal intensity. Therefore, we anticipate that these r-GO-AuNRs are a potential multifunctional nanomaterial that can be used for sensitive disease diagnosis, as vehicles for therapeutic drug delivery, and for NIR-sensitive photothermal therapy.[23]

EXPERIMENTAL SECTION

Preparation of Optically Reduced r-GO-AuNRs. To prepare r-GO-AuNRs using the optical method, 10 mL of GO-AuNR solution (OD 1.0 at 230 nm, 0.125 mg/mL) containing 100 μL of ammonium hydroxide (28%, w/v) was placed in a Pyrex glass reactor equipped with a water-circulating jacket to maintain the solution temperature at 25 °C (Figure S2). Next, the solution was irradiated with a Xe lamp (power density, 1.56 W/cm^2) for 120 min. After illumination for 120 min, the solutions were centrifuged to remove the ammonium hydroxide.

Instrumental Setup for Photoacoustic Imaging. Photoacoustic images were visualized using a commercial ultrasound scanner equipped with a SonixTouch research package (Ultrasonix Corp., Vancouver, BC, Canada). Ultrasound transducers with operating frequency ranges of 2−5, 5−14, and 8−40 MHz were connected to the scanner. A Nd:YAG laser excitation system (Surelite III-10 and Surelite OPO Plus, Continuum Inc., Santa Clara, CA, USA) was used to produce laser pulses whenever the Q-switch trigger was activated by a function generator (AFG3252, Tektronix Corp., Beaverton, OR, USA). The pulse repetition rate was 10 Hz, and the pulse length was 5−7 ns. Laser irradiation was performed using a homemade optic fiber bundle (Fiberoptic System, Inc., Simi Valley, CA, USA) that bifurcated on both sides of the US transducer (Figure S4a).

***In Vitro* Evaluation of PA Performance.** To evaluate the PA contrast intensities, Tygon tubes laid across the center of a water bath were imaged (Figure S4b). For wavelength-dependent PA imaging (680, 700, 720, 740, 760, 780, or 800 nm), a Nd:YAG laser system with an average energy density of 6.2 mJ/cm^2 was used. A linear array US transducer with an operating frequency range of 5−14 MHz was used as the PA signal detector. The distance between the array transducer and the Tygon tube was fixed at 30 mm, which was equal to the laser focal depth. To analyze (1) the effect of laser power strength (4.2, 5.2, 6.2, 7.2, or 8.2 mJ/cm^2) on PA contrast intensity and (2) the effect of AuNR, GO-AuNR, or r-GO-AuNR concentration on PA contrast intensity under a constant irradiation power (6.2 mJ/cm^2), laser pulses (740 nm) were delivered, and the resultant PA signals were detected using a single US transducer. To analyze the effect of bandwidth frequency on the amplification of the PA signal, three different kinds of US transducers were used (convex array transducer, range 2−5 MHz; linear array transducer, range 5−14 MHz; and linear array transducer, range 8−40 MHz). The optimal imaging depth depended on the US transducer. Thus, a focal depth of 30 mm was used for the 2−5 and 5−14 MHz transducers, whereas a depth of 20 mm was used for the 8−40 MHz transducer. Photoacoustic signals were acquired during laser irradiation, and PA images were reconstructed by averaging 128 sequential frames, thus improving the signal-to-noise ratio. Photoacoustic image reconstruction was conducted using the coherence factor-based sound speed correction method.[32] After selecting the regions of interest in the reconstructed images, the intensities of the PA images were calculated using MATLAB.

***In Vivo* PA Imaging.** All animal experiments performed in this study were approved by the Sogang University Animal Studies Committee. To analyze the contrast intensity and the PA images achieved with r-GO-AuNRs, GO-AuNRs, or AuNRs, equal concentrations of AuNRs (optical density, around 1.0 au) were mixed with Matrigel (50%, v/v). Each mixture (100 μL) was then administered by subcutaneous injection into 4-week-old female Balb/C mice. The parameters for *in vivo* PA imaging were as follows: pulse repetition frequency, 10 Hz; pulse length, 5−7 ns; and imaging depth, 30 mm. The laser pulses had wavelengths of 750 nm because the maximum optical absorption of r-GO-AuNRs occurs at this wavelength. The same US transducer, with an operating frequency range of 5−14 MHz, was used to detect both US and PA signals. Geographic confirmation of the target site was conducted using US images prior to laser irradiation. Image reconstruction and the calculation of PA contrast intensities were performed as in the *in vitro* experiments.

FDTD Simulations. A linearly (x) polarized plane wave (λ = 750 nm) was simulated on the gold nanorod structures (aspect ratio = 3.5). The empirical dielectric constants of gold, as reported by Rakic,[33] Johnson, and Christy, were used with interpolation. The relative permeability of gold was assumed to be $\mu_r = 1$, and the dielectric constant was defined as $\varepsilon_{Au}(\lambda) = n^2 - k^2$. By adopting the Maxwell−Garnett formalism, the dielectric constants of air, graphene oxide, and reduced graphene oxide were determined to be $\varepsilon = 1.002$, $\varepsilon = 1.767\,541$, and $\varepsilon = 1.7689$, respectively.

Conflict of Interest: The authors declare no competing financial interest.

Supporting Information Available: Materials, experimental details including synthesis, and characterization. This material is available free of charge *via* the Internet at http://pubs.acs.org.

Acknowledgment. This work was supported by the National Research Foundation of Korea (NRF-2013R1A1A1061387 and NRF-2013R1A1A2056165).

REFERENCES AND NOTES

1. Wang, X.; Pang, Y.; Ku, G.; Xie, X.; Stoica, G.; Wang, L. V. Noninvasive Laser-Induced Photoacoustic Tomography for Structural and Functional *in Vivo* Imaging of the Brain. *Nat. Biotechnol.* **2003**, *21*, 803–806.
2. Wang, L. H. V.; Hu, S. Photoacoustic Tomography: *In Vivo* Imaging from Organelles to Organs. *Science* **2012**, *335*, 1458–1462.
3. Wilson, K.; Homan, K.; Emelianov, S. Biomedical Photoacoustics beyond Thermal Expansion Using Triggered Nanodroplet Vaporization for Contrast-Enhanced Imaging. *Nat. Commun.* **2012**, *3*, 618–627.
4. Ku, G.; Wang, X.; Stoica, G.; Wang, L. V. Multiple-Bandwidth Photoacoustic Tomography. *Phys. Med. Biol.* **2004**, *49*, 1329–1338.
5. de la Zerda, A.; Bodapati, S.; Teed, R.; May, S. Y.; Tabakman, S. M.; Liu, Z.; Khuri-Yakub, B. T.; Chen, X.; Dai, H.; Gambhir, S. S. Family of Enhanced Photoacoustic Imaging Agents for High-Sensitivity and Multiplexing Studies in Living Mice. *ACS Nano* **2012**, *6*, 4694–4701.
6. Eghtedari, M.; Oraevsky, A.; Copland, J. A.; Kotov, N. A.; Conjusteau, A.; Motamedi, M. High Sensitivity of *in Vivo* Detection of Gold Nanorods Using a Laser Optoacoustic Imaging System. *Nano Lett.* **2007**, *7*, 1914–1918.

7. Mallidi, S.; Larson, T.; Tam, J.; Joshi, P. P.; Karpiouk, A.; Sokolov, K.; Emelianov, S. Multiwavelength Photoacoustic Imaging and Plasmon Resonance Coupling of Gold Nanoparticles for Selective Detection of Cancer. *Nano Lett.* **2009**, *9*, 2825–2831.
8. Wilson, K.; Homan, K.; Emelianov, S. Biomedical Photoacoustics beyond Thermal Expansion Using Triggered Nanodroplet Vaporization for Contrast-Enhanced Imaging. *Nat. Commun.* **2012**, *3*, 618–627.
9. Song, K. H.; Kim, C. H.; Cobley, C. M.; Xia, Y. N.; Wang, L. V. Near-Infrared Gold Nanocages as a New Class of Tracers for Photoacoustic Sentinel Lymph Node Mapping on a Rat Model. *Nano Lett.* **2009**, *9*, 183–188.
10. Kim, J. W.; Galanzha, E. I.; Shashkov, E. V.; Moon, H. M.; Zharov, V. P. Golden Carbon Nanotubes as Multimodal Photoacoustic and Photothermal High-Contrast Molecular Agents. *Nat. Nanotechnol.* **2009**, *4*, 688–694.
11. Chen, Y. S.; Frey, W.; Kim, S.; Kruizinga, P.; Homan, K.; Emelianov, S. Silica-Coated Gold Nanorods as Photoacoustic Signal Nanoamplifiers. *Nano Lett.* **2011**, *11*, 348–354.
12. De La Zerda, A.; Zavaleta, C.; Keren, S.; Vaithilingam, S.; Bodapati, S.; Liu, Z.; Levi, J.; Smith, B. R.; Ma, T. J.; Oralkan, O.; Cheng, Z.; Chen, X. Y.; Dai, H. J.; Khuri-Yakub, B. T.; Gambhir, S. S. Carbon Canotubes as Photoacoustic Molecular Imaging Agents in Living Mice. *Nat. Nanotechnol.* **2008**, *3*, 557–562.
13. Chen, Y.-S.; Frey, W.; Kim, S.; Homan, K.; Kruizinga, P.; Sokolov, K.; Emelianov, S. Enhanced Thermal Stability of Silica-Coated Gold Nanorods for Photoacoustic Imaging and Image-Guided Therapy. *Opt. Express* **2010**, *18*, 8867–8878.
14. Lim, D. K.; Barhoumi, A.; Wylie, R. G.; Reznor, G.; Langer, R. S.; Kohane, D. S. Enhanced Photothermal Effect of Plasmonic Nanoparticles Coated with Reduced Graphene Oxide. *Nano Lett.* **2013**, *13*, 4075–4079.
15. Ming, T.; Zhao, L.; Chen, H.; Woo, K. C.; Wang, J.; Lin, H.-Q. Experimental Evidence of Plasmophores: Plasmon-Directed Polarized Emission from Gold Nanorod−Fluorophore Hybrid Nanostructures. *Nano Lett.* **2011**, *11*, 2296–2303.
16. Marcano, D. C.; Kosynkin, D. V.; Berlin, J. M.; Sinitskii, A.; Sun, Z.; Slesarev, A.; Alemany, L. B.; Lu, W.; Tour, J. M. Improved Synthesis of Graphene Oxide. *ACS Nano* **2010**, *4*, 4806–4814.
17. Robinson, J. T.; Tabakman, S. M.; Liang, Y.; Wang, H.; Casalongue, H. S.; Vinh, D.; Dai, H. Ultrasmall Reduced Graphene Oxide with High Near-Infrared Absorbance for Photothermal Therapy. *J. Am. Chem. Soc.* **2011**, *133*, 6825–6831.
18. Dreyer, D. R.; Park, S.; Bielawski, C. W.; Ruoff, R. S. The Chemistry of Graphene Oxide. *Chem. Soc. Rev.* **2010**, *39*, 228–240.
19. Ng, Y. H.; Iwase, A.; Kudo, A.; Amal, R. Reducing Graphene Oxide on a Visible-Light $BiVO_4$ Photocatalyst for an Enhanced Photoelectrochemical Water Splitting. *J. Phys. Chem. Lett.* **2010**, *1*, 2607–2612.
20. Liang, Y. Y.; Wu, D. Q.; Feng, X. L.; Mullen, K. Dispersion of Graphene Sheets in Organic Solvent Supported by Ionic Interactions. *Adv. Mater.* **2009**, *21*, 1679–1683.
21. Li, D.; Muller, M. B.; Gilje, S.; Kaner, R. B.; Wallace, G. G. Processable Aqueous Dispersions of Graphene Nanosheets. *Nat. Nanotechnol.* **2008**, *3*, 101–105.
22. Dinesh, K.; S, K.; Dong-Kwon, L. Plasmon-Assisted and Visible-Light Induced Graphene Oxide and Efficient Fluorescence Quenching. *Chem. Commun.* **2014**, *50*, 13481–13484.
23. Feng, L.; Wu, L.; Qu, X. New Horizons for Diagnostics and Therapeutic Applications of Graphene and Graphene Oxide. *Adv. Mater.* **2013**, *25*, 168–186.
24. Huang, L.; Liu, Y.; Ji, L.-C.; Xie, Y.-Q.; Wang, T.; Shi, W.-Z. Pulsed Laser Assisted Reduction of Graphene Oxide. *Carbon* **2011**, *49*, 2431–2436.
25. Gilje, S.; Dubin, S.; Badakhshan, A.; Farrar, J.; Danczyk, S. A.; Kaner, R. B. Photothermal Deoxygenation of Graphene Oxide for Patterning and Distributed Ignition Applications. *Adv. Mater.* **2010**, *22*, 419–423.
26. Chen, L. C.; Wei, C. W.; Souris, J. S.; Cheng, S. H.; Chen, C. T.; Yang, C. S.; Li, P. C.; Lo, L. W. Enhanced Photoacoustic Stability of Gold Nanorods by Silica Matrix Confinement. *J. Biomed. Opt.* **2010**, *15*, 016010-1–016010-6.
27. Pu, K. Y.; Shuhendler, A. J.; Jokerst, J. V.; Mei, J. G.; Gambhir, S. S.; Bao, Z. N.; Rao, J. H. Semiconducting Polymer Nanoparticles as Photoacoustic Molecular Imaging Probes in Living Mice. *Nat. Nanotechnol.* **2014**, *9*, 233–239.
28. Link, S.; Burda, C.; Nikoobakht, B.; El-Sayed, M. A. Laser-Induced Shape Changes of Colloidal Gold Nanorods Using Femtosecond and Nanosecond Laser Pulses. *J. Phys. Chem. B* **2000**, *104*, 6152–6163.
29. McGahan, J. P.; Goldberg, B. B. *Diagnostic Ultrasound*, 2nd ed.; Informa Healthcare: New York, 2008; p 52.
30. Zhu, Y.; Murali, S.; Cai, W.; Li, X.; Suk, J. W.; Potts, J. R.; Ruoff, R. S. Graphene and Graphene Oxide: Synthesis, Properties, and Applications. *Adv. Mater.* **2010**, *22*, 3906–3924.
31. Bitounis, D.; Ali-Boucetta, H.; Hong, B. H.; Min, D.-H.; Kostarelos, K. Prospects and Challenges of Graphene in Biomedical Applications. *Adv. Mater.* **2013**, *25*, 2258–2268.
32. Yoon, C.; Kang, J.; Han, S.; Yoo, Y.; Song, T.-K.; Chang, J. H. Enhancement of Photoacoustic Image Quality by Sound Speed Correction: *Ex Vivo* Evaluation. *Opt. Express* **2012**, *20*, 3082–3090.
33. Rakic, A. D.; Djurisic, A. B.; Elazar, J. M.; Majewski, M. L. Optical Properties of Metallic Films for Vertical-Cavity Optoelectronic Devices. *Appl. Opt.* **1998**, *37*, 5271–5283.